 doi:10.20944/preprints202011.0074.v4

Article

Synthesis, Structural Characterization, and Biological Activities of Organically Templated Cobalt Phosphite (H2DAB)[Co(H2PO3)4]·2H2O

Najlaa Hamdi [1], Souad Chaouch [1], Ivan da Silva [2], Mohamed Ezahri [3], Mohammed Lachkar [1], Rama Alhasan [4], Ahmad Yaman Abdin [4], Claus Jacob [4] and Brahim El Bali [1*]

[1] Engineering Laboratory of Organometallic and Molecular Materials, Faculty of Sciences, University Sidi Mohamed Ben Abdellah, Po. Box 1796 (Atlas), 30000 Fez, Morocco; hamdi.najlae@gmail.com (N.H.); chaouch2005@yahoo.fr (S.C.); lachkar.mohammed@gmail.com (M.L.); b_elbali@yahoo.com (B.E.B.)
[2] ISIS Facility, STFC Rutherford Appleton Laboratory, Chilton, Oxfordshire OX11 0QX, UK; ivan.da-silva@stfc.ac.uk
[3] Laboratoire Matériaux et Environnement, Faculté des Sciences, Université Ibn Zohr, B.P. 8106, Cité Dakhla, 80000 Agadir, Maroc; m.ezahri@uiz.ac.ma
[4] Division of Bioorganic Chemistry, School of Pharmacy, Saarland University, D-66123 Saarbruecken, Germany; s8rralh@stud.uni-saarland.de (R.A.); yaman.abdin@uni-saarland.de (A.Y.A.); c.jacob@mx.uni-saarland.de (C.J.)
* Correspondence: b_elbali@yahoo.com (B.E.)

Abstract: A novel hybrid cobalt phosphite, (H2DAB)[Co(H2PO3)4]·2H2O, has been synthesized by using slow evaporation method, in the presence of cobalt nitrate, phosphorous acid and 1,4- diaminobutane (DAB= 1,4- diaminobutane) as a structure-directing agent. Single crystal X-ray diffraction analysis showed that the compound crystallizes in the P-1(n.2) triclinic space group, with the following unit cell parameters (Å, °) a = 5.4814 (3), b = 7.5515 (4), c = 10.8548 (6), α = 88.001 (4), β = 88.707 (5), γ = 85.126 (5), and V= 447.33 (4) Å3. The crystal structure was built up from corner-sharing [CoO6] octahedra, forming chains parallel to [001], which are interconnected by H2PO3 pseudo-tetrahedral units. The deprotonated cations, residing between the parallel chains, interacted with the inorganic moiety via hydrogen bonds leading thus to the formation of the 3D crystal structure. The Fourier transform infrared spectrum showed characteristic bands corresponding to the phosphite group and the organic amine. The thermal behavior of the compound consisted mainly of the loss of its organic moiety and the water molecules. The biological tests exhibited significant activity against *Candida albicans* and *Escherichia coli* strains in all used concentrations, while less inhibitory activity was pronounced against *Staphylococcus epidermidis* and *Saccharomyces cerevisiae*, and in the case of multi-cellular organisms, no activity against the nematode model *Steinernema feltiae* was detected.

Keywords: Hybrid phosphite; X-Ray crystal structure; FTIR; Thermal behavior; Biological activities; Antimicrobial; micro-organisms;

1. Introduction

Hybrid organic-inorganic compounds have attracted a great deal of attention in different fields because of their rich structural chemistry and wide potential applications in ion-exchange, adsorption, separation, and catalysis [1–7]. Within this class of structures, hybrid phosphite remains as an important focus of many material scientists due to the wide, and sometimes novel, range of structures exhibiting various architectures and dimensionality [8]. Such resulting martials can either be simple (single metal) [9–12], mixed-metal [13–20] or hybrid (organic-inorganic) [21,22]. In this context, we describe in the present manuscript the synthesis, crystal structure, spectroscopic characterization via Fourier

 doi:10.20944/preprints202011.0074.v4

transform infrared (FTIR) analysis, and thermal behavior of the new hybrid phosphite (H2DAB)[Co(H2PO3)4]·2H2O. Moreover, we also report on the biological activity of the compound, against *C. albicans, E. coli strains, S. epidermidis, and S. cerevisiae*.

In the next section, we shall lay out the experimental setting regarding the synthesis, characterization and biological evaluation. In section 3, we opted to conjoin the results and the discussion. The section reports and discusses the structure of the organically templated cobalt phosphite synthesized, the results from the infrared spectroscopy, thermal behaviors of the compound and, finally the biological activity against the different organisms mentioned above. In the last section we conclude.

2. Materials and Methods

2.1. Materials and Instrumentation

All reagents were acquired from commercial sources and used without further purification. The infrared spectrum of the compound was recorded on a VERTEX 70 FTIR Spectrometer in the range 4000–400 cm^{-1} using the ATR technique at 4 cm^{-1} resolutions. Thermogravimetric analysis (TGA) data were recorded on an SDT-Q600 analyzer from TA Instruments (Eschborn, Germany). The temperature varied from RT to 1273.15 K at a heating rate of $10°/min^{-1}$. Measurements were carried out on samples in open platinum crucibles under air flow.

2.2. Synthesis

Individual crystals of $(H_2DAB)[Co(H2PO3)4]·2H2O$ were synthesized under ambient conditions. The reaction mixture of $Co(NO_3)_2·6H_2O$ (1 mmol, 300 mg), 1,4-diaminobutane (DAB) (1.92 mmol, 170 mg), and H_3PO_3 (3.65 mmol, 300 mg) was shaken in distilled water for 6h and then left at room temperature to cool. After 2 weeks, hexagonal purple crystals arised on the bottom of the beaker, were harvested, washed with water-ethanol mixture (80:20) and dried in air.

2.3. Crystal Structure Determination

Single-crystal X-ray diffraction measurement was carried out at room temperature using an Agilent Gemini S diffractometer equipped with a CCD detector and molybdenum (Mo) radiation source. Acquired data was processed with the CrysAlisPro software [23]. Using Olex2 [24], the structure was solved with the olex2.solve [25] structure solution program using Charge Flipping and refined with the olex2.refine [25] refinement package using Gauss-Newton minimization. All non-hydrogen atoms were refined anisotropically, and hydrogen atoms were included in the model at calculated positions, refined with a rigid model with their Uiso value fixed at 1.2Ueq of their parent atoms.

Table 1 reports the crystallographic data and experimental details of data collection and structure refinements. The structural graphics were created using both DIAMOND program [26] and Mercury [27].

Table 1. Experimental X-ray data collection from $(H_2DAB)[Co(H_2PO_3)_4]·2H2O$.

Chemical Formula	$(C4H_{14}N_2)[Co(H_2PO_3)_4]·2H_2O$
Mr (g/mol)	*509.08*
F(000)	263.9
Symmetry, S.G.	Triclinic P-1 (n. 2)
Cell parameters / V	A = 5.4814 (3) Å, b = 7.5515 (4) Å, c = 10.8548 (6)Å, α = 88.001 (4)°, β = 88.707 (5)°, γ = 85.126 (5)° / 447.33 (4) $Å^3$
Z	1
λ (Mo Kα radiation) (Å)	0.71073

 doi:10.20944/preprints202011.0074.v4

T(K)/μ(mm^{-1})	298 / 1.39
Crystal size (mm)	0.25 × 0.25 × 0.3
Measured reflections / independent reflections (reflections with I ≥ 2u(I)) / parameters	9480 / 2005 (1878) / 137
θmin − θmax (°) / Rint	1.9–27.8/0.024
Reciprocal space limiting indices	h: −6–7, k: −9–9, l: −13–14
R[F2 > 2σ(F2)] / wR(F2) / G.O.F.	0.026 / 0.072 / 1.03

Supplementary tables of crystal structure and refinement, the full list of bond lengths and angles, and anisotropic thermal parameters were deposited with the Inorganic Crystal Structure Database, FIZ, Hermann von Helmholtz Platz 1, 76344 Eggenstein Leopoldshafen, Germany; fax: (+49) 7247 808 132; Email: crysdata@fiz-karlsruhe.de. Deposition number is CCDC 1882579.

2.4. Biological assays

2.4.1. The Antimicrobial Activity

The activity of $(H_2DAB)[Co(H_2PO_3)_4]\cdot 2H_2O$ compound against *Escherichia coli*, *Staphylococcus epidermidis*, *Candida albicans*, and *Saccharomyces cerevisiae* was investigated in routine microbial growth assays based on optical density and recorded in the form of growth curves. Fresh cultures of *S. epidermidis*, *E. coli*, *C. albicans*, and *S. cerevisiae* were prepared on bacterial tryptic soy broth, Luria-Bertani broth (LB), Sabouraud Dextrose Agar (SDA), and Yeast Peptone Dextrose (YPD) agar media, respectively. After 18–24 h of incubation, the microbial colonies from these Agar plates were then transferred into 10 mL solution of 0.9% *w/v* NaCl (saline), and the turbidity of the suspension was adjusted to 0.5 of McFarland standard. These microbial suspensions were then exposed to the samples as described below. Bacterial and yeast culture with growth medium were employed as negative control, sterile distilled water was utilized as solvent control, while the positive control consisted of a mixture of 10,000 units/mL of penicillin, 10,000 μg/mL of streptomycin, and 25 μg/mL of amphotericin B. The sample was evaluated at various dilutions (of 250, 500, and 1000 μM), and the plates were incubated at 37 °C for 24 h. Microbial growth was monitored by recording the optical density of the samples at 0 h and 24 h, using a Micro Plate Reader E800 at 593 nm. These absorbance values were converted into percentages and compared to the negative control whose absorbance values were normalized to 100% and served as references at each time interval. All experiments were carried out in triplicate at three different occasions (n = 9). Results are represented as mean ± SD, and statistical significances were calculated by one-way ANOVA using GraphPad Prism (Version 5.03, GraphPad Software, La Jolla, CA, USA) with $p < 0.05$ considered to be of statistical significance.

2.4.2. Nematocidal Activity

The model nematode *Steinernema feltiae* was purchased from Sautter und Stepper GmbH (Ammerbuch, Germany) in the form of powder and stored at 4 °C in the dark. Fresh samples were utilized prior to each experiment. A homogeneous mixture was prepared by dissolving 200 mg of nematode powder in 50 mL distilled water. Later, the nematode suspension was placed for 15 min at room temperature with shaking and in moderate light. Viability was examined under a light microscope at four-fold magnification (TR 200, VWR International, Leuven, Belgium). The viability of nematodes above 80% in each sample was considered a prerequisite for each experiment. Ten microliters of nematode suspension were added to each well of a 96-well plate. The hybrid cobalt phosphite $(H_2DAB)[Co(H_2PO_3)_4]\cdot 2H_2O$ was then added into the wells to achieve final concentrations of 250, 500, and 1000 μM. Afterward, the final volume in each well was adjusted to 100 μL

Preprints (www.preprints.org) | NOT PEER-REVIEWED | Posted: 22 November 2021 doi:10.20944/preprints202011.0074.v4

by adding Phosphate Buffered Saline (PBS pH = 7.4). PBS and ethanol (10 µL per well) were employed as negative and positive controls, respectively, and sterile distilled water was the solvent control. Each experiment was performed independently on three different occasions and in triplicate (n = 9). Living and dead nematodes were counted under the microscope prior to treatment, and the viability fraction (V0) was calculated (usually >0.9). Then, 50 µL of lukewarm water (40 °C) was added to each well to stimulate the nematodes prior to counting. After 24 h, the V24 fraction was calculated, by once more counting the living and dead nematodes, and expressed as a percentage of initial viability V0 according to the equation:

$$\text{Viability (\%)} = [V_{24}/V_0] \times 100$$

Results are represented as mean ± SD, and GraphPad Prism (Version 5.03, GraphPad Software, La Jolla, CA, USA) was used to calculate the statistical significances by one-way ANOVA. $p < 0.05$ was statistically significant.

3. Results and Discussion

3.1. Structural Description

As shown in Figure 1, there is one crystallographically distinct Co located at special position (½ 0 ½) (Table 1). The asymmetric unit of $(H_2DAB)[Co(H_2PO_3)_4]\cdot 2H_2O$, which contains 13 non-hydrogen atoms located on general positions (Table 1), including 1 water oxygen named O(13). Cobalt cation shows octahedral geometry, coordinating six oxygen atoms from adjacent phosphite groups. The Co–O bond lengths range from 2.0919(12) Å to 2.1336(12) Å (Table 3), with an average Co–O distance of 2.1258 Å, in good agreement with the value 2.113 Å reported in $[(C_4N_8H_{12})Co(HPO_3)_2(C_2O_4)_3]$ [28] and to that of 2.1205 Å for $(C_2H_{10}N_2)[Co_3(HPO_3)_4]$ [29]. All $(H_2PO_3)^-$ units adopt pseudo-tetrahedral coordination geometry. P(5) shares two oxygen with adjacent Co atoms, while P(7) is connected by one P–O–Co bond and possesses a short terminal P–O bond (1.4955 (15) Å). The P–O bond distances are in the range 1.5050(13)–1.5732(14) Å for P(5) atom [$d_{(P\text{-}O)}$Av. 1.5283 Å] and 1.4987(13)–1.5625(15) Å for P(7) [$d_{(P\text{-}O)}$Av. 1.5189 Å]. P(5) and P(7) atoms have a terminal phosphite P–H bond 1.241 (1) and 1.3127 (1) Å, respectively. These values are in good agreement with those reported in $(C_2NH_8)_2[Co_3(HPO_3)_4]$, $(C_4N_2H_{12})[Co(HPO_3)_2]$ [30], and $(H_2dab)_{0.5}Co(H_2PO_3)(C_2O_4)$[31].

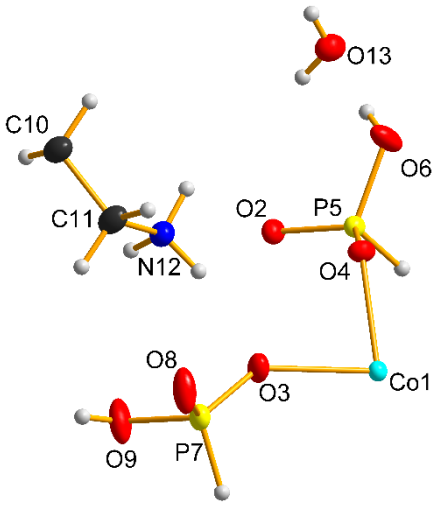

Figure 1. Asymmetric unit of $(H_2DAB)[Co(H_2PO_3)_4]\cdot 2H_2O$. Thermal ellipsoids are shown at 60% probability.

The strict alternation of $[CoO_6]$ octahedra and $[H_2PO_3]^-$ pseudo tetrahedral via oxygen vertices results in an anionic network with a Co/P ratio of 1/2. The polyhedral units are

Preprints (www.preprints.org) | NOT PEER-REVIEWED | Posted: 22 November 2021 doi:10.20944/preprints202011.0074.v4

joined through corners sharing four-membered rings, which are thereby connected through their edges forming an infinite one-dimensional chain rising along [100], Figure 2.

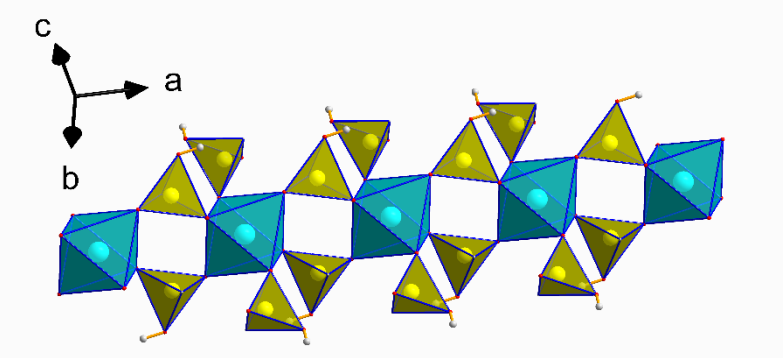

Figure 2. A fragment of the structure of $(H_2DAB)[Co(H_2PO_3)_4]\cdot 2H_2O$ along [010], showing the infinite four-membered ring chain propagating along [100]. Polyhedrons: cyan [CoO_6], yellow [H_2PO_3].

The individual chain units are further linked together through hydrogen bond interactions (Figure 3, Table 4). The 1,4-butanediammonium templates, made up by N12, C11, C10 atoms and their symmetry-related $N12^i$, $C11^i$ and $C10^i$, which resides between the parallel chains, are deprotonated. They are further ensuring, together with the free-standing water molecules, the stability of the three-dimensional network.

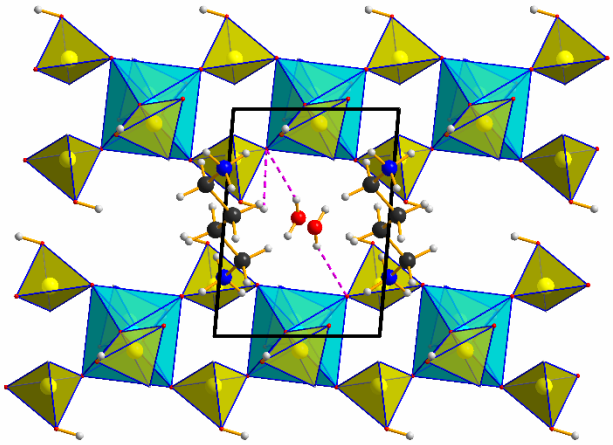

Figure 3. The crystal structure of $(H_2DAB)[Co(H_2PO_3)_4]\cdot 2H_2O$ in a projection along c-axis emphasizing the hydrogen bonds (dashed lines).

Table 4. Hydrogen bonding network in the framework of $(H_2DAB)[Co(H_2PO_3)_4]\cdot 2H_2O$

D-H···A	D-H / Å	H···A / Å	D···A / Å	DHA / °
O6-H6···O13	0.80 (3)	1.80 (3)	2.605 (2)	175 (3)
O9-H9···O8	0.82 (1)	1.77 (1)	2.574 (2)	169(1)
N12-H12A···O6	0.89 (1)	2.16 (1)	2.900 (2)	140 (1)
N12-H12B···O3	0.89 (1)	2.02 (1)	2.887 (2)	166 (1)
N12-H12C···O8	0.89 (1)	1.91 (1)	2.776 (2)	165 (1)
O13-H13A···O2	0.71 (3)	2.22 (3)	2.888 (2)	159 (3)
O13-H13B···O4	0.76 (3)	2.11 (3)	2.863 (2)	179 (4)

3.2. Infrared Spectroscopy

Preprints (www.preprints.org) | NOT PEER-REVIEWED | Posted: 22 November 2021 doi:10.20944/preprints202011.0074.v4

The infrared spectrum of $(H_2DAB)[Co(H_2PO_3)_4]\cdot 2H_2O$ (Figure 4) exhibits bands corresponding to the vibration modes of the organic template, phosphite groups and water molecules. The stretching vibration of NH_2 in 1,4-butanediammonium cation is observed in the high frequencies 3090–3200 cm^{-1}, while its bending appears at 1600 cm^{-1} [32]. The values pointing between 2600-2736 cm^{-1} correspond to the symmetric and asymmetric stretching of $(NH3)^+$, and it also confirms the protonation form of the organic amine molecule. The two large vibration at around 2813 and 2923 are boil down to the stretching mode of υ(-CH2-), while the medium band at 1314 cm^{-1} coincide with the stretching vibration of υ(C–N). The characteristic bond of phosphite groups is manifested by a small and medium vibration at around 2420 and 2430 cm^{-1} and it corresponds to the stretching vibration of υ(P–H), as well as the bands from 990 to 1030 cm^{-1} are assigned to the bending mode of δ(P–H). The vibration modes centered at 1057 and 1164 cm^{-1} are ascribed to the symmetric and asymmetric stretching of PO_3 group, while its symmetric and asymmetric bending are observed at 670 and 460 cm^{-1}, respectively. The broad vibration located at 916 cm^{-1} is attributed to the stretching vibration of P–OH bond [20]. The set of bands related to the stretching vibration and deformation of the OH group and belonging to water molecules is observed at around 3000 and 1645 cm^{-1} [33, 34].

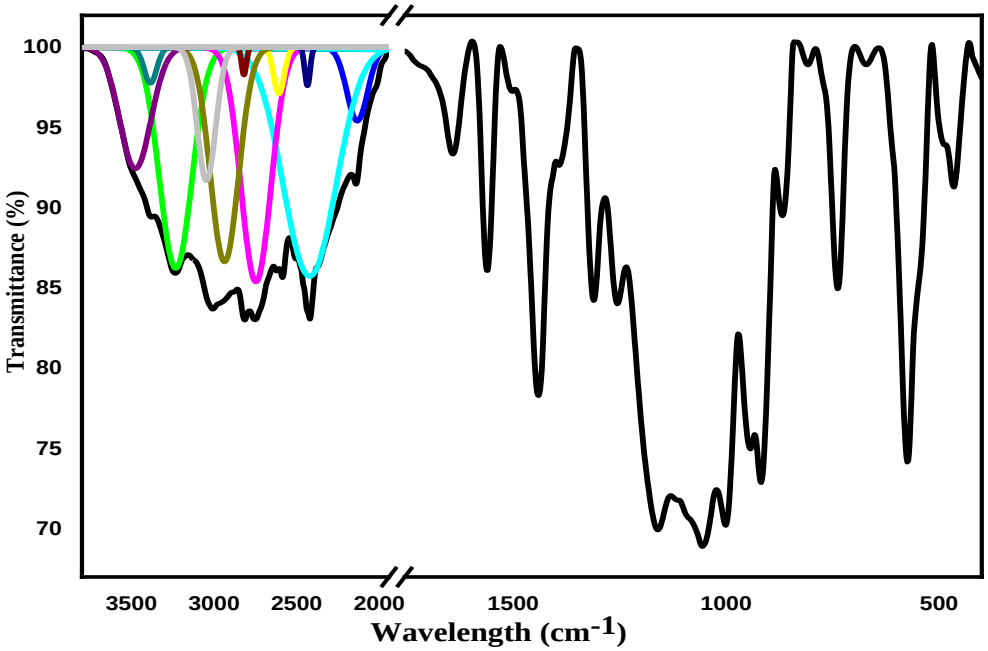

Figure 4. Infrared spectrum of $(H_2DAB)[Co(H_2PO_3)_4]\cdot 2H_2O$.

3.3. Thermal Behavior

Thermal analysis was performed under air atmosphere, and as depicted in figure 5, the experimental data of $(H_2DAB)[Co(H2PO3)4]\cdot 2H2O$ showed four separated stages of weight loss in a total of 52.75% from 25 to 1000 °C. The first experimental mass loss (5.45%), occurred between 150 and 270 °C, corresponds to the easy departure of one and half molecule of the two structural water molecules (Calculated value 5.30%). This quick dehydration of the hybrid cobalt-phosphite, may be explained by the engagement of the water molecules in a weak network of hydrogen bonds. This variation is coupled with a sharp exothermic signal in the differential thermal analysis trace at 174 °C. The second weight loss of 5.35%, ranging from 271 to 358 °C on TG curve, was related to the departure of the remaining half water molecule and the release of NH_3 unit from the organic moiety (Calculated value 5.11%). This degradation was manifested by an exothermic intense peak at 292 °C. The experimental value of 8.95%, pointing at 385 °C on TG profile and highlighted by a small set of signals on DTA measurement, coincided with the continuous volatilization of the organic moiety (Calculated value 8.85%). The last and final

Preprints (www.preprints.org) | NOT PEER-REVIEWED | Posted: 22 November 2021 doi:10.20944/preprints202011.0074.v4

experimental mass loss (33%), observed between 497 and 973 °C, can be associated with the total degradation of the organic moiety and the formation of the Cobalt metaphosphate compound $Co(PO_3)_2$ through a condensation reaction of phosphite groups (Calculated value 37%). This formation was mainly characterized by a small exothermic heat flow at 632 °C.

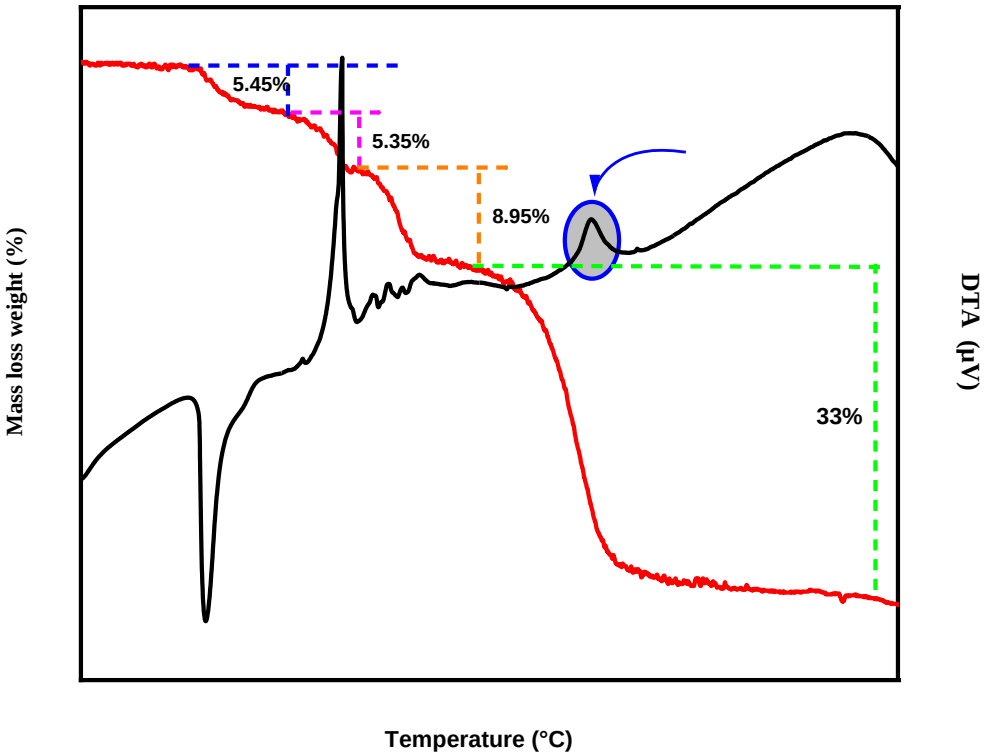

Figure 5. Thermogravimetric (TG) and differential thermal analysis (TDA) curves of $(H_2DAB)[Co(H_2PO_3)_4]\cdot 2H_2O$.

3.4. Biological Activities

The hybrid cobalt phosphite compound was tested for its antimicrobial activity against two bacteria (*Escherichia coli* and *Staphylococcus epidermidis*) and two Fungi (*Saccharomyces cerevisiae* and *Candida albicans*) strains. A mixture of 10,000 units/mL of penicillin, 10,000 µg/mL of streptomycin, and 25 µg/mL of Amphotericin B was used as a control at three different concentration 250, 500, 1000 µg/mL. Ethanol was used as a positive control.The percentage inhibition and minimum inhibitory concentration (MIC) values of the compound based on the growth of microorganisms are shown in Figure 6.

Preprints (www.preprints.org) | NOT PEER-REVIEWED | Posted: 22 November 2021 doi:10.20944/preprints202011.0074.v4

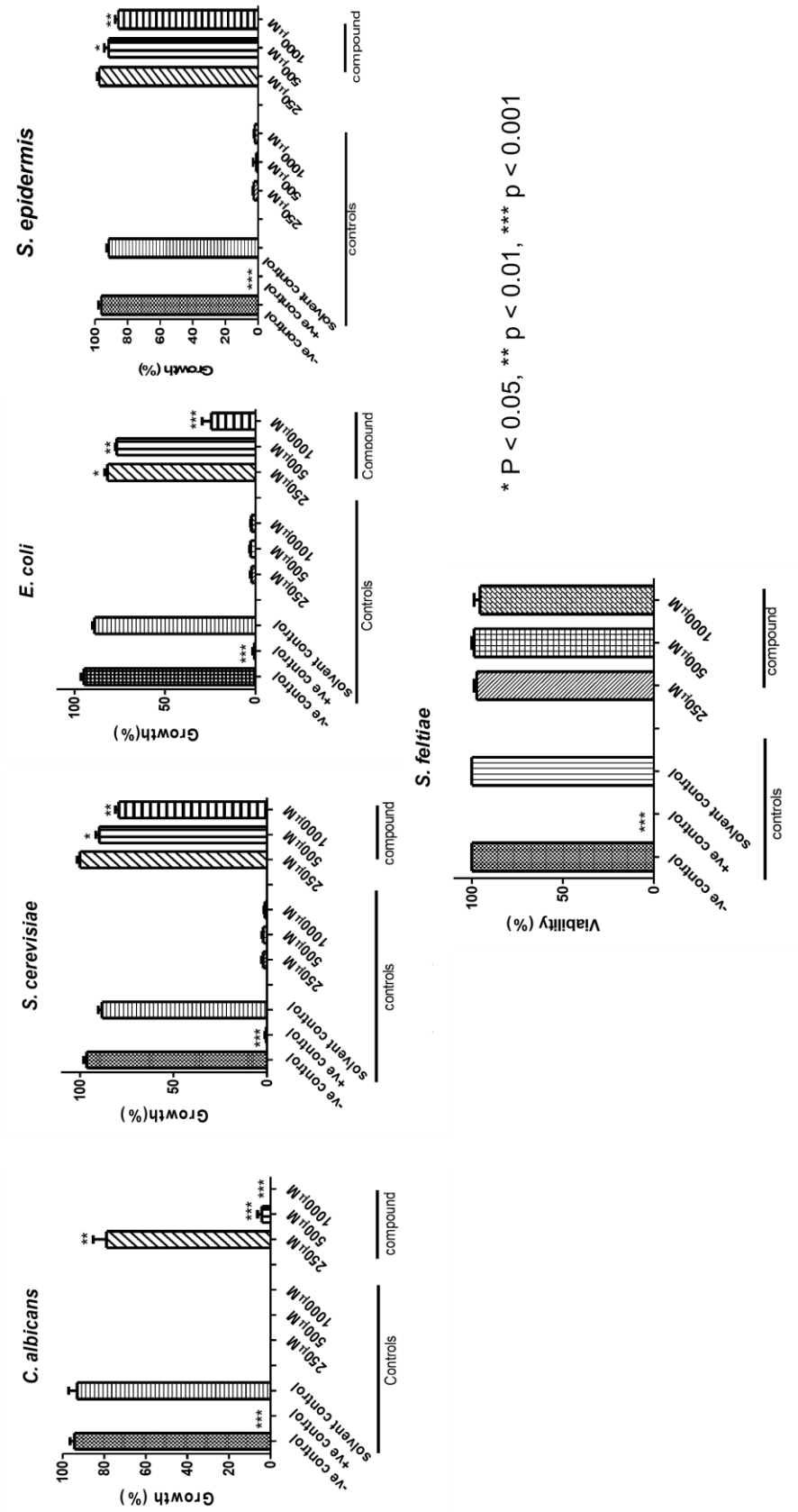

Figure 6. Antibacterial activity of $(H_2DAB)[Co(H_2PO_3)_4]\cdot 2H_2O$ against *Candida albicans, Saccharomyces cerevisiae, Escherichia coli, Staphylococcus epidermidis* and *Steinernema feltiae*.

Statistically, the compound exhibited significant inhibitory activity against *Candida albicans, Saccharomyces cerevisiae, Escherichia coli, Staphylococcus epidermidis* but not the

 doi:10.20944/preprints202011.0074.v4

multi-cellular organism *Steinernema feltiae*. In terms of observed growth reduction, the hybrid cobalt phosphite compound demonstrated strong antifungal activity against *C. albicans* at an MIC value of 500 and 1000 $\mu g \cdot mL^{-1}$. The inhibition of growth, however, was much less in the case of *S. cerevisiae*. The compound showed lower activity as antibacterial agent. The *E. coli* media demonstrated higher inhibition that *S. epidermidis*. The nematode assay showed that the compound had almost no impact on viability.

5. Conclusions

A novel organically templated cobalt phosphite (H2DAB)[Co(H2PO3)4]·2H2O has been synthesized using wet chemistry. Single crystal structure analysis revealed that the framework displays a chain-like structure, containing vertex sharing four-membered rings formed by the connectivity between CoO6 octahedrons and [H2PO3]-pseudo-tetrahedral units bound through their edges. The diprotonated 1,4-butanediammonium acts as a stabilizer of the inorganic network through hydrogen bonds. The thermogravimetric analysis showed that the dehydration of the hybrid phosphite takes place in three steps, resulting mainly from the loss of the organic moiety and water molecules. The antimicrobial investigation showed significant activity against all the microorganisms utilized except for S. feltiae. Further studies on hybrid phosphite compound are needed to assess their safety and applicability in the fields of medicine and agriculture.

Supplementary Materials: The following are available online at www.mdpi.com/xxx/s1, Figure S1: title, Table S1: title, Video S1: title.

Author Contributions: Investigation, Najlaa Hamdi, Souad Chaouch, Ivan da Silva, Mohamed Ezahri and Rama Alhasan; Project administration, Brahim El Bali; Supervision, Mohammed Lachkar , Claus Jacob and Brahim El Bali; Visualization, Ivan da Silva, Rama Alhasan and Brahim El Bali; Writing – original draft, Najlaa Hamdi, Souad Chaouch and Ivan da Silva; Writing – review & editing, Ahmad Yaman Abdin and Brahim El Bali.

Funding: This research had no external funding.

Institutional Review Board Statement: Not applicable.

Informed Consent Statement: Not applicable.
Data Availability Statement: All the data generated from this study is available upon request. Please contact the corresponding author.

Acknowledgments: The authors would like to acknowledge the support and technical assistance of Interface Regional University Center (Sidi Mohammed Ben Abdellah University, Fez) and National Center for Scientific and Technical Research (CNRST-Rabat). Mrs. Alhasan would like to acknowledge Dahye Kim and Hyemin Oh from Ewha Womans University (South Korea) for their assistance in the biological activity's tests.

Conflicts of Interest: The authors declare no conflict of interest

References

1. Garcia-Fernandez, A.; Bermudez-Garcia, J.M.; Castro-Garcia, S.; Artiaga, R.; Lopez-Beceiro, J.; Senaris-Rodriguez, M.A.; Sanchez-Andujar, M. Dielectric properties induced by the framework in the hybrid organic-inorganic compounds M(dca)2pyz M= Fe, Co and Zn. *Polyhedron* **2016**, *114*, 249–255.
2. Xiong, D.B.; Li, M.R.; Liu, W.; Chen, H.H.; Yang, X.X.; Zhao, J.T. Synthesis, structure and luminescence property of two lanthanum phosphite hydrates: La-2(H_2O)(x)(HPO_3)(3) (x=1,2). *J. Solid State Chem.* **2006**, *179*, 2571–2577.
3. Wang, L.; Song, T.; Fan, Y.; Tian, Z.; Wang, Y.; Shi, S.; Xu, J. Synthesis and characterization of a new open-framework fluorinated gallium phosphite with three-dimensional intersecting channels. *J. Solid State Chem.* **2006**, *179*, 3400–3405.
4. Hamdi, N.; Hidaoui, S.; Hassani, H. O.; Lachkar, M.; Dusek, M.; Morley, N.; El Bali, B. Synthesis, crystal structure, physical and catalytic oxidation studies of a new hybrid phosphate [$(N_2H_5)_2Co(HPO_4)_2$]. *J.Mol. Struct*. **2020**, 1217, 128317.

5. Shi, S.H.; Qian, W.; Li, G.H.; Wang, L.; Yuan, H.M.; Xu, J.N.; Zhu, G.S.; Song, T.Y.; Qiu, S.L. Building three-dimensional metal phosphites from the corner-shared four-membered rings chain. *J. Solid State Chem.* **2004**, *177*, 3038–3044.
6. Lin, Z.E.; Fan, W.; Gao, F.; Chino, N.; Yokoi, T.; Okubo, T. A novel layered bimetallic phosphite intercalating with organic amines: Synthesis and characterization of $Co(H_2O)_4Zn_4(HPO_3)_6.C_2N_2H_{10}$. *J. Solid State Chem.* **2006**, *179*, 723–728.
7. Zhong, Y.J.; Chen, Y.M.; Sun, Y.Q.; Yang, G.Y. Syntheses and characterization of two new zinc phosphites with 1D chains decorated by Zn-centered complexes. *J. Solid State Chem.* **2005**, *178*, 2613–2619.
8. Agarwal, R.A.; Mukherjee, S. One dimensional coordination polymers of Cd(II) and Zn(II): Synthesis, structure, polar packing through strong inter-chain hydrogen bonding and gas adsorption studies. *Polyhedron* **2016**, *106*, 163–170.
9. Ouarsal, R.; Tahiri, A.A.; El Bali, B.; Lachkar, M.; Bolte, M. Strontium dihydrogenphosphite. *Acta Crystallogr.* **2002**, *E58*, i19–i20.
10. Ouarsal, R.; Tahiri, A.A.; Lachkar, M.; Slimani, Z.; El Bali, B.; Bolte, M. Barium dihydrogen phosphate hemihydrates. *Acta Crystallogr.* **2002**, *E58*, i72–i73.
11. Chaouche, S.; Ouarsal, R.; El Bali, B.; Lachkar, M.; Bolte, M.; Dusek, M. $Li_2HPO_3\ H_2O$: Crystal Structure and IR Spectrum. *J. Chem Crystallogr.* **2010**, *40*, 526–530.
12. El Bali, B.; Massa, W. Redetermination of copper(II) hydrogenphosphite dehydrate. *Acta Crystallogr.* **2002**, *E58*, i29–i31.
13. Chaouch, S.; Ouarsal, R.; Akouibaa, M.; Rakib, S.; Lachkar, M.; El Bali, B.; Dusek, M. $Cs_2[M(H_2O)_6]_3(HPO_3)_4$, M= Co, Ni: Crystal structures, IR and thermal studies. *J. Phys. Conf. Ser.* **2018**, *984*, 12–15.
14. Ouarsal, R.; Tahiri, A.A.; El Bali, B.; Lachkar, M.; Harrison, W.T.A. Sodium zinc tris(dihydrogenphosphite) hydrate $NaZn(H_2PO_3)_3.H_2O$. *Acta Crystallogr.* **2002**, *E58*, i23–i25.
15. Ouarsal, R.; Tahiri, A.A.; Lachkar, M.; Dusek, M.; Fejfarová, K.; El Bali, B. Sodium magnesium tris(dihydrogenphosphite)monohydratehydrate, $NaMg(H_2PO_3)_3\ H_2O$. *Acta Crystallogr.* **2003**, *E59*, i33–i35.
16. Ouarsal, R.; Essehli, R.; Lachkar, M.; Zenkouar, M.; Dusek, M.; Fejfarová, K.; El Bali, B. Dipotassium cobalt(II) bis(hydrogenphosphite) dihydrate, $K_2Co(HPO_3)_2{,}2H_2O$. *Acta Crystallogr.* **2004**, *E60*, i66–i68.
17. Messouri, I.; El Bali, B.; Capitelli, F.; Piniella, J.F.; Lachkar, M.; Slimani, Z. Diammoniumtris[hexaaquamagnesium(II)]tetrakis[hydrogenphosphate(III)], $(NH_4)_2[Mg(H_2O)_6]_3(HPO_3)_4$. *Acta Crystallogr.* **2005**, *E61*, i129–i131.
18. Ouarsal, R.; El Bali, B.; Lachkar, M.; Dusek, M.; Fejfarová, K. Diammoniumtris[hexaaquanickel(II)]tetrakis[hydrogenphosphate(III)], $(NH_4)_2[Ni(H_2O)_6]_3(HPO_3)_4$. *Acta Crystallogr.* **2005**, *E61*, i171–i173.
19. Ouarsal, R.; El Bali, B.; Lachkar, M.; Dusek, M.; Fejfarová, K. Diammonium tris[hexaaquacobalt(II)] tetrakis[hydrogenphosphate(III)], $(NH_4)_2[Co(H_2O)_6]_3(HPO_3)_4$. *Acta Crystallogr.* **2005**, *E61*, i168–i170.
20. Ouarsal, R.; Lachkar, M.; Dusek, M.; Albert, E.B.; Castelló, J.B.C.; El Bali, B. Crystal structure of $NaCd(H_2PO_3)_3\ H_2O$ and spectroscopic study of $NaM(H_2PO_3)_3\ H_2O$, M = Mn, Co, Ni, Zn, Mg and Cd. *Polyhedron*. **2016**, *106*, 132–137.
21. Chaouche, S.; Ouarsal, R.; Lachkar, M.; Capitelli, F.; El Bali, B. Crystal Structure and IR Study of $(C_6H_5NH_3)[ZnCl(HPO_3)]$. *J. Chem Crystallog.* **2010**, *40*, 486–490.
22. Suhua, S.; Wei, Q.; Guanghua, L.; Li, W.; Hongming, Y.; Jianing, X.; Zhu, G.; Song, T.; Qiu, S.J. Building three-dimensional metal phosphites from the corner-shared four-membered rings chain. *Solid State Chem.* **2004**, *177*, 3038–3044.
23. *CrysAlisPro Software System*, version 1.171.38.41; Rigaku Corporation: Oxford, UK, 2015.
24. Dolomanov, O.V.; Bourhis, L.J.; Gildea, R.J.; Howard, J.A.K.; Puschmann, H. OLEX2: A complete structure solution, refinement and analysis program. *J. Appl. Cryst.* **2009**, *42*, 339–341.
25. Bourhis, L.J.; Dolomanov, O.V.; Gildea, R.J.; Howard, J.A.K.; Puschmann, H. The anatomy of a comprehensive constrained, restrained refinement program for the modern computing environment—*Olex2* dissected. *Acta Cryst. A* **2015**, *71*, 59–75.
26. Brandenburg, K.; Putz, H. *DIAMOND Version 3*; Crystal Impact GbR: Bonn, Germany, 2005.

27. Macrae, C.F.; Bruno, I.J.; Chisholm, J.A.; Edgington, P.R.; McCabe, P.; Pidcock, E.; Rodriguez-Monge, L.; Taylor, R.; Van de Streek, J.; Wood, P.A. Mercury CSD 2.0—New Features for the Visualization and Investigation of Crystal Structures. *J. Appl. Cryst.* **2008**, *41*, 466–470.
28. Mandal, S.; Natarajan, S. Inorganic–organic hybrid structure: Synthesis, structure and magnetic properties of a cobalt phosphite–oxalate, $[C_4N_2H_{12}][Co_4(HPO_3)_2(C_2O_4)_3]$. *J. Solid State Chem.* **2005**, *178*, 2376–2382.
29. Fernandez, S.; Pizarro, J. L.; Mesa, J. L.; Lezama, L.; Arriortua, M. I.; Rojo, T. Hydrothermal synthesis of a new layered inorganic–organic hybrid cobalt (II) phosphite:$(C_2H_{10}N_2)[Co_3(HPO_3)_4]$: crystal structure and spectroscopic and magnetic properties. *Int.J. Inorg. Mat*. **2001**, 3, 331-336.
30. Liu, X.; Xing, Y.; Liu, X. Solvothermal synthesis and magnetic properties of cobalt(II) phosphite structures of varying dimensionality. *Cryst. Eng. Commun*. **2010**, *12*, 383–386.
31. Li, J.; Li, T.; Zeng, H.; Zou, G.; Lin, Z. Solvent-free synthesis of inorganic-organic hybrid solids with chainlike, layered, and open-framework structures. *Inorg Chem Comm*, **2018**, 95, 8-11.
32. Kantarcı, Z.; Sag lam, S.; Kasap, E. Vibrational spectroscopic studies on the 1,4-diaminobutane-T_d-type clathrates: $Cd(dabn)M(CN)_4{\cdot}1{,}5C_6H_6$ (M=Cd or Hg). *Spectrosc. Lett.* **2002**, *35*, 811–819.
33. Novak, A. Hydrogen bonding in solids correlation of spectroscopic and crystallographic data. In *Large Molecules. Structure and Bonding*; Springer: Berlin/Heidelberg, Germany, 1974; pp. 177–216.
34. Gilli, G.; Gilli, P. Towards a Unified Hydrogen-Bond Theory. *J. Mol. Struct.* **2000**, *552*, 1–15.